Available online at www.sciencedirect.com
SCIENCE DIRECT
Journal of Power Sources 155 (2006) 311–318
JOURNAL OF POWER SOURCES
www.elsevier.com/locate/jpowsour

Feasibility study of a mini fuel cell to detect interference from a cellular phone

M.O. Abdullah*, Y.K. Gan

Mechanical and Manufacturing System Engineering, Faculty of Engineering, Universiti Malaysia Sarawak, 94300 Kota Samarahan, Sarawak, Malaysia

Received 14 April 2005; accepted 9 May 2005
Available online 11 July 2005

Abstract

Fuel cells produce electricity without involving combustion processes. They generate no noise, vibration or air pollution and are therefore suitable for use in many vibration-free power-generating applications. In this study, a mini alkaline fuel cell signal detector system has been designed, constructed and tested. The initial results have shown the applicability of such system for used as an indicator of signal disturbance from cellular phones. A small disturbance even at 4 mV cm^{-1}, corresponding to an amplitude of 12–18 mG in terms of electromagnetic field, can be well detected by such a device. Subsequently, a thermodynamics model has been developed to provide a parametric study by simulation to show the likely performance of the fuel cell alone in other environments. As such the model can provide many useful generic design data for alkaline fuel cells. Two general conclusions can be drawn from the present theoretical study: (i) fuel cell performance increases with temperature, pressure and correction factor, C_f; (ii) the temperature factor (E/T) increases with increasing temperature and with increasing pressure factor.

Keywords: Signal detector; Alkaline fuel cell; Signal disturbance; Environmental health; Cellular phone

1. Introduction

A fuel cell is an electrochemical device that produces electricity via inverse electrolysis. A chemical reaction and electrical charge transfer occurs within the fuel cell. This is very similar to the way a battery produces electricity. Unlike a battery, a fuel cell produces electricity as long as there is a continuous supply of fuel. No combustion however, nor noise generation takes place in the fuel cell.

The aforesaid advantages have encouraged the application of fuel cells in the signal sensing applications. For instance, Kim et al. [1] used a polymer electrolyte membrane (PEM) fuel cell for the detection of ethanol gas concentration. A two-electrode sensor cell for CO detection in a hydrogen-rich gas had been investigated by Planje et al. [2]. Fuel cell sensors for breath testing and environmental monitoring by gas discrimination have been investigated by Bull et al. [3]. These efforts have encouraged the present application for signal detection in cellular phones.

With the growing interest in fuel cells, the alkaline fuel cell (AFC) is said to be one of the most promising candidates [4]. The long lifetime and the possibility to use non-noble catalysts [4–6] give it advantages over other types of fuel cell system. It is considered that the kinetics of oxygen reduction is superior in an alkaline solution than in acid, which allows the use of less expensive catalysts to obtain an equivalent reaction rate [3,7]. Also, compared with other fuel cells, the reaction in the AFC occurs at a relatively low temperature.

The number of anecdotal reports of symptoms experienced by hand-phone users due to electromagnetic effects and the low-level radio frequency fields around the world is increasing [8–10]. These symptoms include headaches, dizziness, warmth or tingling around the ear and face, and difficulties in concentrating, see Chia et al. [8]. It is believed

* Corresponding author. Tel.: +60 82 679301; fax: +60 82 672 317.
E-mail address: amomar@feng.unimas.my (M.O. Abdullah).

0378-7753/$ – see front matter © 2005 Elsevier B.V. All rights reserved.
doi:10.1016/j.jpowsour.2005.05.013

Nomenclature

AFC	alkaline fuel cell
C_f	overall cell gain/loss factor, $C_f = (nF/\Delta S)(\partial E/\partial E)_P$ from Eq. (6b)
E	voltage
EMF	electromotive force or 'theoretical' open-circuit voltage of a cell determined under convention-defined standard conditions
E/T	temperature factor
E^0	EMF at standard pressure and temperature
F	Faraday constant, the charge on one mole of electrons, 96,485 C mol^{-1}
G	Gibbs free energy
$\bar{h}_f$	enthalpy of formation per mole
H	enthalpy
$\ln(P_2/P_1)$	pressure factor
n	number of cells in a fuel cell stack
PEM	polymer electrolyte membrane
r	polarization resistance, $\Omega\,cm^2$
R	molar or 'universal' gas constant, 8314.3 J kg^{-1} mol^{-1}
S	entropy
T	temperature

Greek letters

η_{actual}	cell efficiency
μ_f	fuel utilization coefficient, defined as ratio of mass of fuel reacted in a cell to mass of fuel input

that if such undesired disturbances could be detected, identified and measured, these could provide a better understanding of the hazards. Also, disturbance identification is useful in providing safety control measure, especially at electrical signal-sensitive areas. Standard guidelines and safety limits of electromagnetic exposure allowed in various countries are summarized in Table A1 in Appendix A.

In the present study, an affordable, non-noble material for the construction of AFC electrodes of the AFC has been used. The research does not aim to improve the AFC design or to increase the power density and efficiency, but to investigate its feasibility for small micro-electronic and mechanical signal applications, particularly for mobile phone signal detection. Further to the experimental work, a parametric study based on thermodynamics and sensitivity analysis has been conducted to provide many useful generic design data for the AFC.

2. Theory and hypothesis

2.1. Theory on experimental work

The overall system, as shown in Fig. 1, was designed and built as an extension of previous work [11]. It consists of four main sections, i.e., the AFC, signal induction, signal converter and detection, and recording section. The mini AFC produced the desired direct current. The voltage generated before and after signal disturbance was then sensed by a Pico-oscilloscope. The results were plotted by a computer that used Pico Technology software.

The mini AFC was of the dissolved fuel design. The anode was made from nickel (Appendix A, Table A2), rather than from the usual, relatively expensive, platinum catalyst. The cathode was carbon since it does not take part in any chemical reaction, but allows electrons flow through it. The fuel used was a mixture of potassium of potassium hydroxide (KOH) and methanol solution, in a 75%:25% weight ratio (Table 2).

The electrochemical reaction of an AFC is well known [2–4]. Reduction of oxygen at the cathode and oxidation of hydrogen at the anode produce electrical energy according to the following reaction:

$$2H_2 + O_2 \rightarrow 2H_2O + \text{electrical energy} \quad (1)$$

The reduction of oxygen in an alkaline solution is given by:

$$O_2 + 2H_2O + 4e^- \rightarrow 4OH^- \quad (2)$$

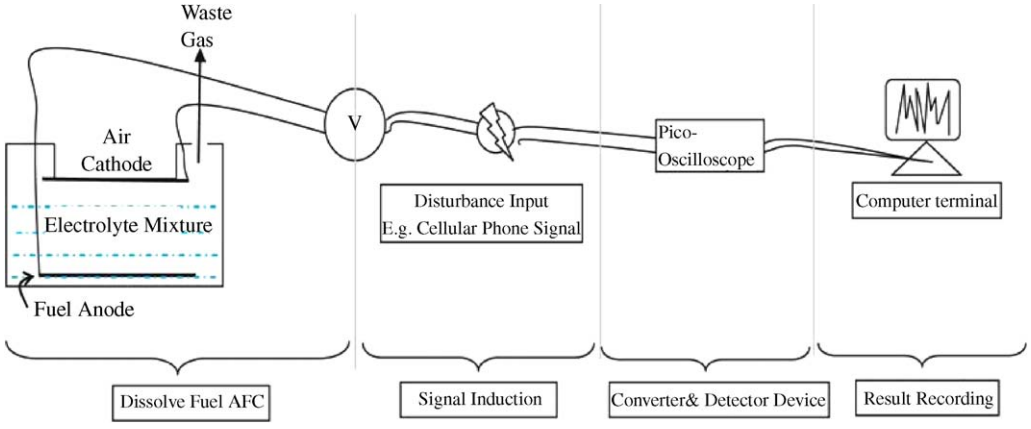

Fig. 1. Schematic diagram of dissolved fuel AFC signal detector.

and the anode reaction, i.e., oxidation of hydrogen, is given by:

$$CH_3OH + 6OH^- \rightarrow 5H_2O + CO_2 + 6e^- \quad (3)$$

2.2. Thermodynamics consideration and sensitivity analysis

The Gibbs free energy available from a fuel cell can be described either in terms of electrical work[1] or the change in enthalpy and entropy[2] as follows:

$$G = -nFE = \Delta H - T\Delta S \quad (4)$$

so that the cell voltage, E, can be evaluated by:

$$E = -\frac{\Delta H - T\Delta S}{nF} = -\frac{\Delta H}{nF} + T\left(\frac{\Delta S}{nF}\right) \quad (5)$$

Differentiating the above equation with respect to T:

$$\left(\frac{\partial E}{\partial T}\right)_P = \frac{\Delta S}{nF} \quad (6a)$$

Now, for an actual fuel cell, a correction factor C_f is introduced to account for the overall cell gains or losses, so that Eq. (6a) becomes:

$$\left(\frac{\partial E}{\partial T}\right)_P = C_f\frac{\Delta S}{nF} \quad (6b)$$

and so:

$$\Delta S = \frac{nF}{C_f}\left(\frac{\partial E}{\partial T}\right)_P \quad (7)$$

The temperature–entropy (T–S) and temperature–etnhalpy (T–H) diagram for H_2 in the region of 130–300 K can be found in Russel [12] and Wolley and Brick [13]. The data extracted from these studies was used to develop Eq. (8) and (9) based on regression method.

The enthalpy–temperature relation was estimated by:

$$H = 14.46T + 3829.36 \quad (8)$$

where H is the enthalpy, J g^{-1} and T is the temperature, °C.

The entropies at different pressure levels as a function of temperature were estimated by:

$$S_{1\,bar} = -1.256E-04T^2 + 5.985E-02T + 60.468 \quad (9a)$$

$$S_{3\,bar} = 2.930E-04T^2 - 4.186E-04T + 64.277 \quad (9b)$$

$$S_{5\,bar} = -2.093E-05T^2 + 4.44E-02T + 65.013 \quad (9c)$$

$$S_{7\,bar} = -8.371E-06T^3 + 2.093E-03T^2 - 0.125T + 74.385 \quad (9d)$$

where S is the entropy, J gm^{-1} K^{-1} and T in °C.

The fuel cell efficiency can be then calculated by Eqs. (10) and (11), as described by Larminie and Dicks [14]:

$$\text{cell efficiency, } \eta_{actual} = \mu_f\frac{E}{EMF} \times 100\% \quad (10)$$

where μ_f is the fuel utilization coefficient and

$$EMF = \frac{-\Delta\bar{h}_f}{nF} = 1.48\,V(\text{at higher heating value, HHV}) \quad (11)$$

where $\bar{h}_f$ is the enthalpy of formation per mole.

A computer program was written to investigate the effects of various parameters on fuel cell performance on the basis of the equations developed above. The computing steps, are shown in the flow chart presented in Fig. 2.

3. Results and discussion

3.1. Results and discussion on experimental study

The change in polarization resistance with time of the nickel catalyst is given in Fig. 3. The properties of the fuel mixture used and the specification of the Pico-oscilloscope are given in Tables 1 and 2, respectively.

The results obtained from a typical signal experiment were as follows. The signal before the system encountered any disturbance is given in Fig. 4. Before any disturbance signal, the dc voltage from the fuel cell has produced a stable, quasi-linear signal wave, as shown in Fig. 4. The introduction of disturbance signal tends to induce and change the quasi-steady signal wave. This is shown clearly in Fig. 5 where the incoming cellular disturbance is introduced at time 23 s, highlighted by Region A. It is found that a small cellular disturbance at 20 mV corresponding to amplitude of 12 mG in terms of electromagnetic field, is detected by the device arrangement used (Region A). The signal has a time period of around 8 s due to the period of the disturbance introduced.

Table 1
Properties of fuel mixture and potassium hydroxide (KOH)

	Value
Wt.% of KOH	75
Wt.% of CH_3OH	25
Concentration of KOH	4 M

Table 2
Specification of Pico-oscilloscope Model ADC212

Voltage range	±20 mV to ±20 V in 9 ranges
Spectrum range	0–76 Hz (min)
Channels	2 BNC, 1 MΩ ac/dc; 1 BNC external trigger
Accuracy	±1%

[1] In a fuel cell, work is converted from electrochemical energy, through inverse electrolysis, i.e., the change in Gibbs free energy, ΔG to electrical work, $W_{elec} = -nFE$.

[2] Since for a reversible system, the Gibbs free energy, $G = H - TS$.

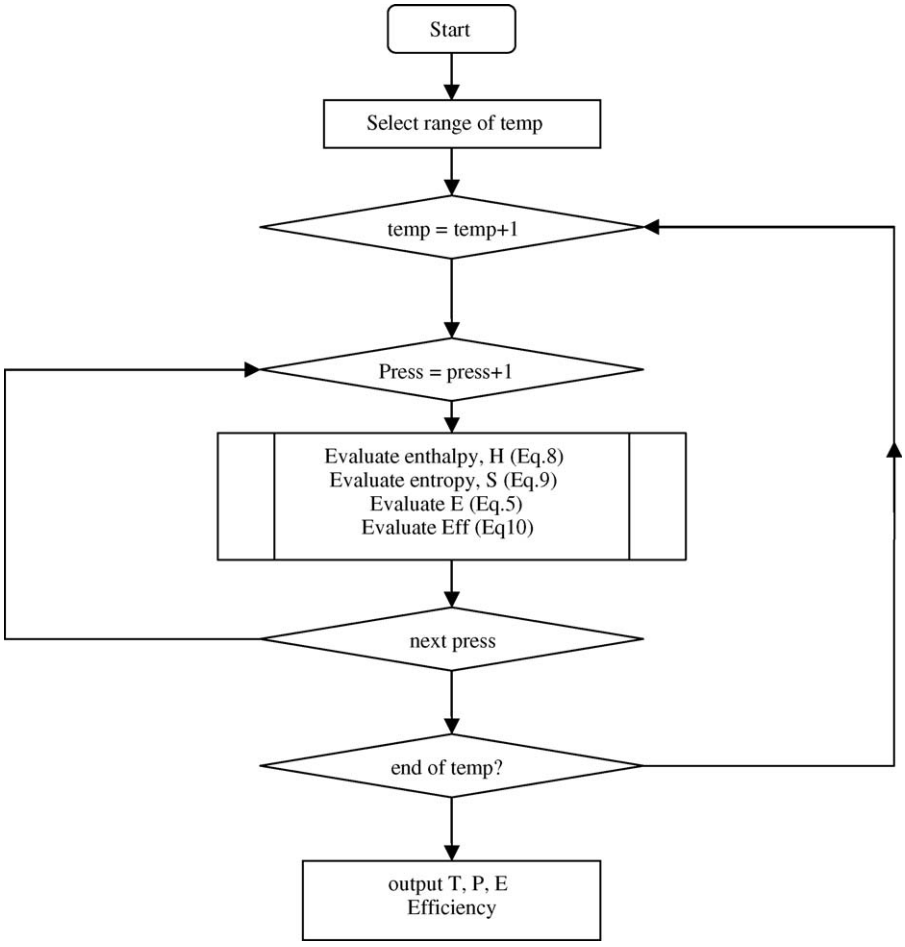

Fig. 2. Flow chart for performance and parametric study of AFC.

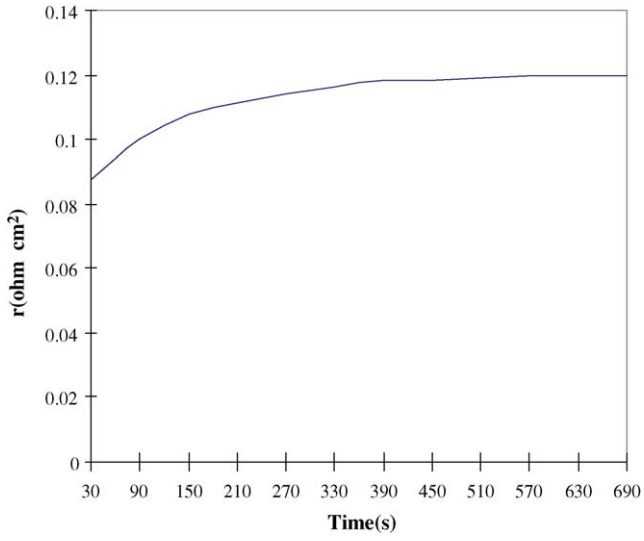

Fig. 3. Plot of polarization resistance of Nickel based electrode vs. time at a constant current load of 1.067 mA cm^{-2}.

Region B is not significant as it indicates a time when the system was shut-off.

3.2. Results and discussion on parametric study

The experimental study reported in the preceding section was undertaken at ambient conditions. Theoretical work was done subsequently, to study the effect of various parameters on fuel cell performance. The aim of the parameteric study was to investigate the thermodynamic perspective as well as the performance of the fuel cell alone if applied at other conditions. The effects of these influencing parameters to the signal disturbance developments are not discussed in this paper. The effect of temperature and pressure on fuel cell performance and at different correction factors, C_f, is presented in Figs. 6–11.

From all the plots, it is apparent that the theoretical voltage and hence efficiency, increases with increasing pressure. A comparison of the influence of the C_f factor, as in Figs. 7–11 show that the fuel cell performance increases with this factor. This is because higher temperatures normally have the advantage of low losses. This is possibly due the fact that transport of H^+ ions from the anode to the cathode increases

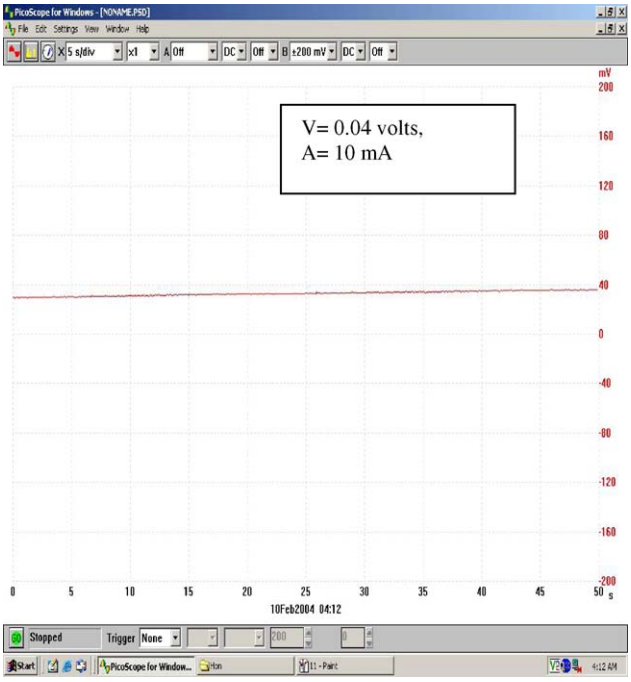

Fig. 4. Before disturbance.

with increasing pressure. The voltage and efficiency increase quite linearly with increasing temperatures. The plots were found to exhibit similar patterns to those reported by Ergul et al. [15] and Ref. [16], which utilized conventional pure platinum electrodes. The comparison plots are presented in Figs. 12 and 13, respectively. Also, as shown in Fig. 13, the overall efficiency increases with pressure.

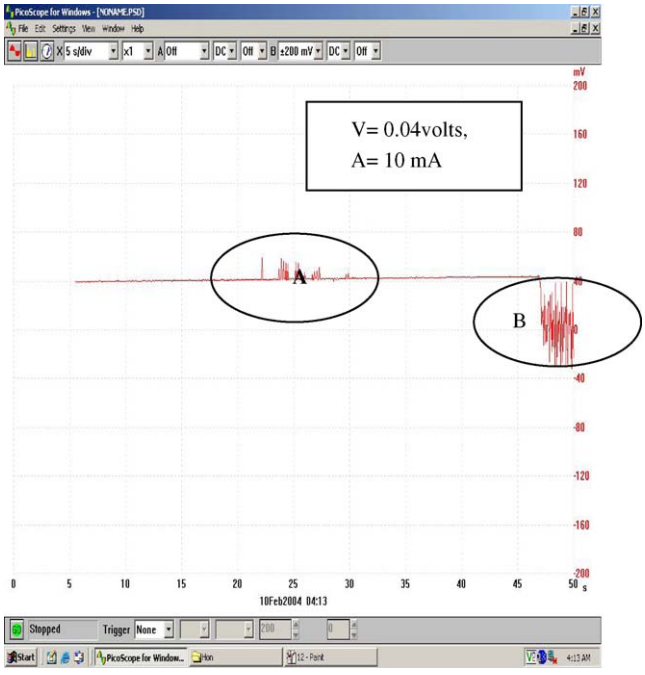

Fig. 5. After disturbance.

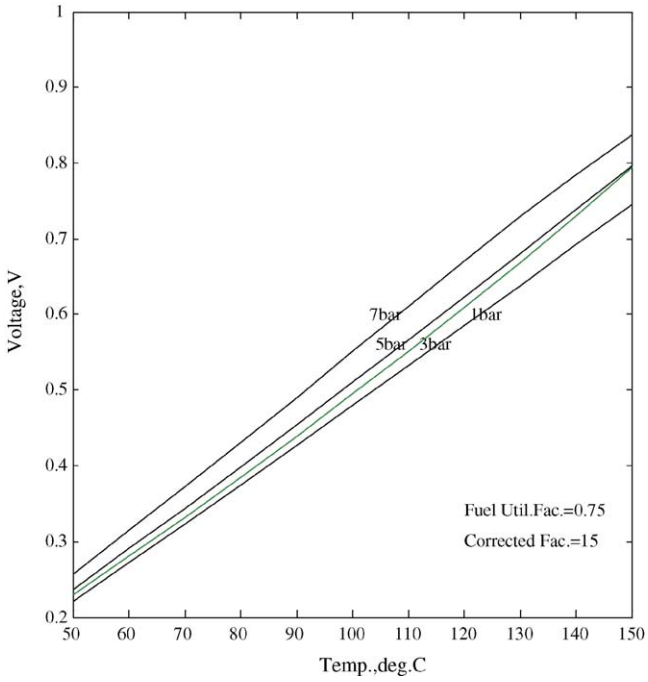

Fig. 6. Theoretical voltage at various temperatures and pressures ($C_f = 15$).

Now, consider the well known Nernst equation which relates the potential generated by an electrochemical cell, E, to the activities a of the chemical species in the cell reaction, $\alpha A + \beta B \leftrightarrow \gamma C + \delta D$, and to the standard potential, E^0, i.e.,

$$E = E^0 + \frac{RT}{nF} \ln \frac{{}^{a}C^{\gamma a} D^{\delta}}{{}^{a}A^{\alpha a} B^{\beta}} \tag{12}$$

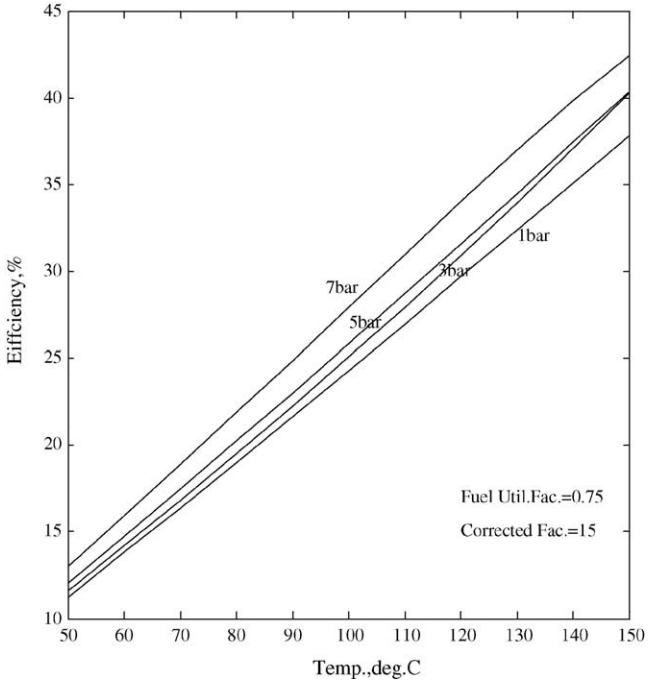

Fig. 7. Theoretical efficiency at various temperatures and pressures ($C_f = 15$).

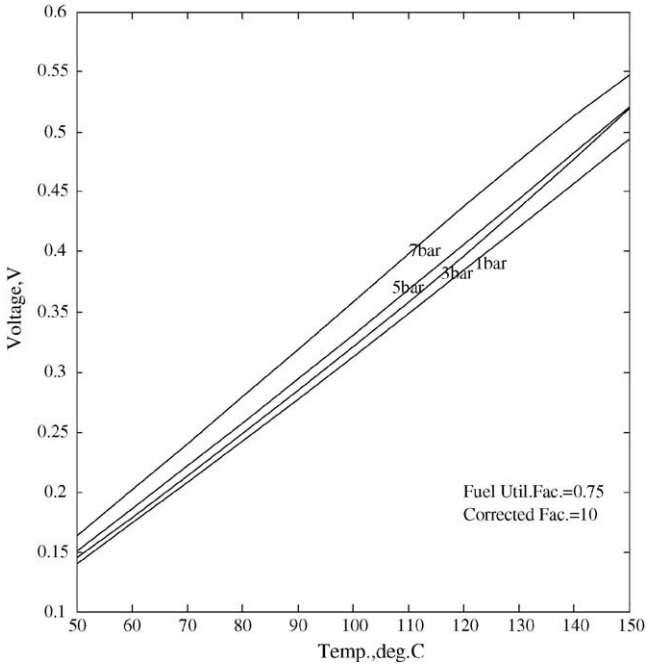

Fig. 8. Theoretical voltage at various temperatures and pressures ($C_f = 10$).

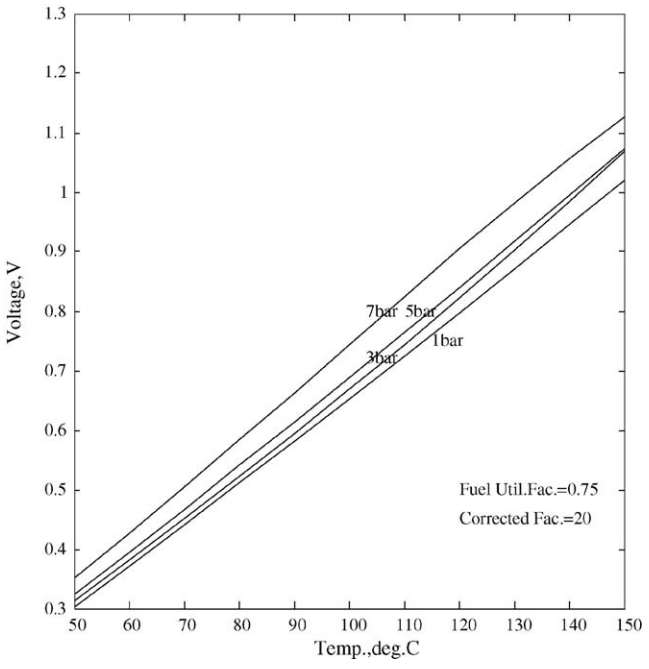

Fig. 10. Theoretical voltage at various temperatures and pressures ($C_f = 20$).

For the present case of the AFC, the following simplified equation can be written:

$$E = E^0 + \frac{RT}{nF} \ln\left(\frac{P_{H_2}}{P_{H_2O}}\right) + \frac{RT}{nF} \ln\left(P_{O_2}\right)^{1/2} \tag{13}$$

where P_{H_2}, P_{O_2} and P_{H_2O} are the partial pressures for hydrogen, oxygen and water, respectively.

Consider only the hydrogen partial pressure and that it changes from P_1 to P_2, Eq. (13) can be reduced to:

$$E \propto \frac{RT}{nF} \ln\left(\frac{P_2}{P_1}\right) \tag{14}$$

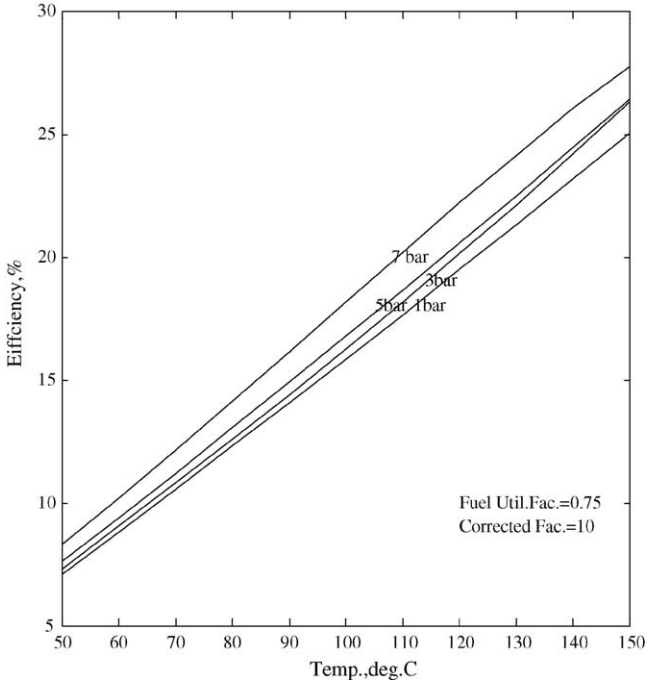

Fig. 9. Theoretical efficiency at various temperatures and pressures ($C_f = 10$).

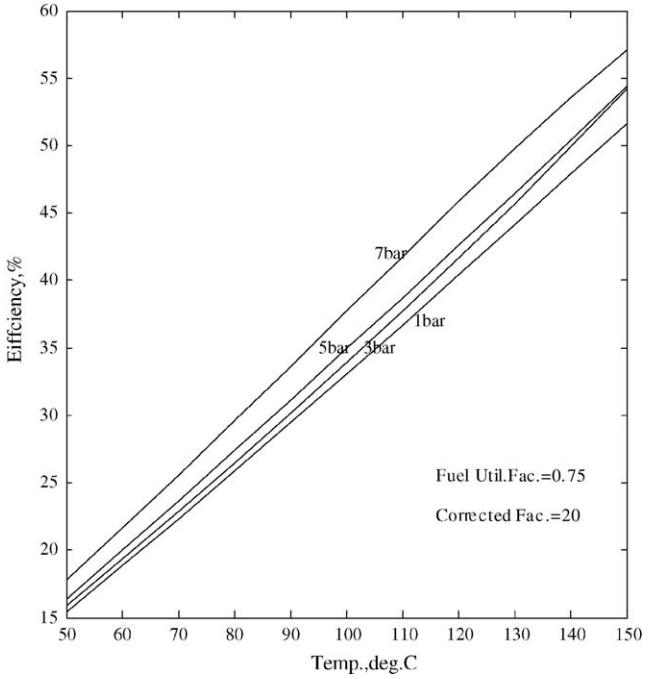

Fig. 11. Theoretical efficiency at various temperatures and pressures ($C_f = 20$).

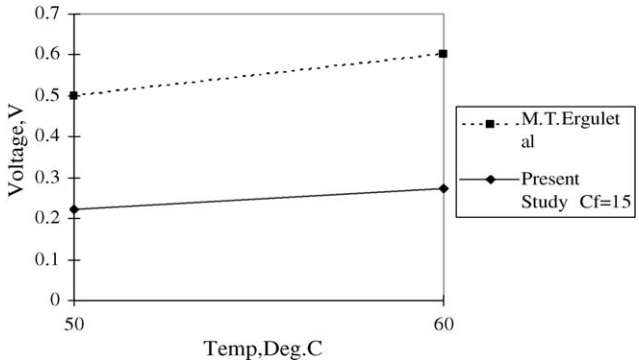

Fig. 12. Comparison of plots of Ergul et al. [15] with present study.

By rearranging,

$$\frac{nF}{R}\underbrace{\left[\frac{E}{T}\right]}_{\text{(temperature factor)}} \cong \ln \underbrace{\left(\frac{P_2}{P_1}\right)}_{\text{(pressure factor)}} \quad (15)$$

Eq. (15) is a partial-dimensionless equation because the temperature factor is not dimensionless.

The computational outputs mentioned earlier in Section 2.2 were rearranged into the form of Eq. (15), with substituted values for the constants $n = 2$, $F = 96{,}485\ \text{C mol}^{-1}$ and $R = 8314.3\ \text{J kg}^{-1}\ \text{mol}$.

A plot of pressure factor ($\ln(P_2/P_1)$) versus temperature factor (E/T) is shown in Fig. 14. The temperature factor (E/T) increases with increasing temperature T. Therefore, this further proves that the fuel cell will have higher performance at higher temperature. Also, an increasing pressure factor at constant temperature increases the performance indicator, i.e., the temperature factor.

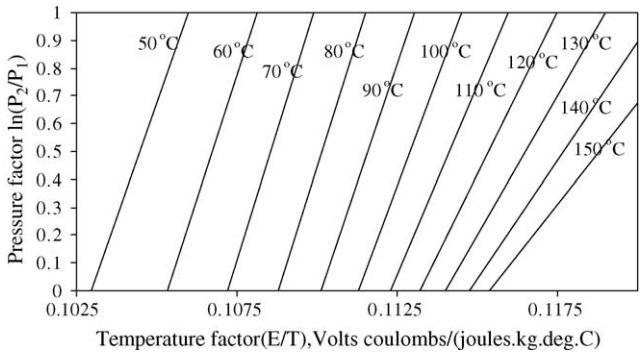

Fig. 14. Performance curves for AFC at various temperatures and pressures.

4. Conclusions

A feasibility study of an affordable fuel cell detecting system has been undertaken via laboratory tests. The anode catalyst was made from nickel, a relatively low-cost material compared with the usual platinum counterpart. The low energy generated by the mini fuel cell can be used for microelectronic or mechanical signal applications. In this study, it is used as a signal indicator of interference from a cellular phone. The results show that a disturbance of 20 mV or 400 mV m^{-1} corresponding to an amplitude of 12–18 mG in terms of electromagnetic field, from the cellular phone. This is below the limit approved by the International Standard (Table A1) in relation to the amplitude of 4 mG in the human body.

A thermodynamics model for parametric study investigation, has been developed to increase the understanding of the inverse electrolysis process and to provide a simple, rational method of predicting the AFC system performance. Simulation of AFC performance demonstrated the model's capability and yielded sensible results (Fig. 14). Two of the general conclusions from the theoretical study are: (i) the fuel cell performance increases with temperature, pressure

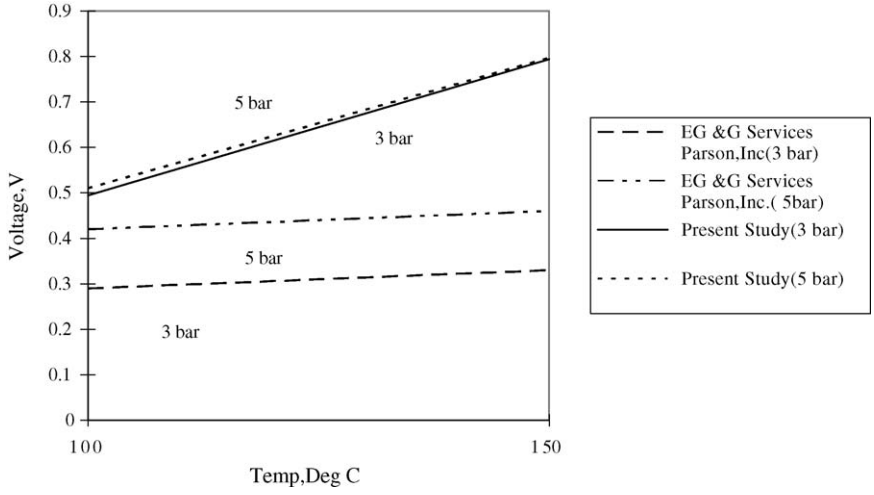

Fig. 13. Comparison plots of Ref. [16] with present study.

Table A1
Standard and guideline limits for continuous exposure published by various organization [9,10]

Standards	Electric field (kV m^{-1})		Magnetic flux density (μT)	
	Public	Occupational	Public	Occupational
ICNIRP (1998)	5	10	0.1	0.5
USA, ACGIH	–	30	–	1
CENELEC (1995)	10	30	0.64	1.6
UK, NRPB	10	10	1.6	1.6
AUS, NH&MRC	5	10	0.1	0.5
Germany (1989)	20.6	20.6	5	5
USSR (1975)	–	5	–	–
USSR (1985)	–	–	–	1.76
Poland (1980)	–	15	–	–

Table A2
Properties of Nickel 200, commercially pure grade (99.6% Ni)

Property	Value
Density (g cm^{-3})	8.89
Melting/range (°C)	1435–1446
Specific heat (J kg^{-1} °C)	456
Thermal conductivity (W m^{-1} °C)	70
Electricity resistivity (Ω m)	0.096×10^{-6}

and correction factor, C_f; (ii) the temperature factor (E/T) increases with increasing temperature and pressure factor.

Acknowledgements

The authors are grateful to K.J. Hon, for assistance with some of the initial experimentation work. Thanks are also to the Faculty technician, Mr. Masri, for his help and contribution in the preliminary testing. The present research work is part of the study funded by the UNIMAS Fundamental Research Grant No. 02-46/434/2004(171).

Appendix A

Standard and guideline limits for continuous exposure published by various organization [9,10], and properties of Nickel 200, commercially pure grade (99.6% Ni) are shown in Tables A1 and A2, respectively.

References

[1] K.C. Kim, S.M. Cho, H.G. Choi, Sens. Actuators 67 (1–2) (2000) 194–198.
[2] W.G. Planje, G.J.M. Janssen, M.P. de Heer, Sens. Actuators 99 (2–3) (2004) 544–555.
[3] D.R. Bull, G.J. Harris, A.B. Ben Rashed, Sens. Actuators 15 (1–3) (1993) 151–161.
[4] T. Burchardt, P. Gouerec, E. Sanchez-Cortezon, Z. Karichev, J.H. Miners, Fuel 81 (2002) 2151–2155.
[5] Y. Kiros, S. Schwartz, J. Power Sources 36 (1991) 547.
[6] Y. Kiros, O. Lindstrøm, T. Kaimakis, J. Power Sources 45 (1993) 219.
[7] W. Vogel, J.T. Lundquist, J. Electrochem. Soc. 117 (1970) 1512.
[8] Chia, Sin-Eng, Hwee-Pin Chia, Jit-Seng Tan, Environ. Health Perspect. 108 (2001) 11.
[9] W.Y. Riadh, Electromagnetic Field and Radiation—Human Bioeffects and Safety, Marcel Dekker, 2002.
[10] National Institute of Environmental Health Science (NIEHS), EMF Exposure Standard, NIEHS, 2002.
[11] Y.K. Gan, Design, construction and experimental work of a mini dissolved fuel alkaline fuel cell for micro-electronic and mechanical signal application. Final year project thesis report, Universiti Malaysia Sarawak, 2004.
[12] C.R. Russel, Elements of Energy Conversion, 4, Pergamon Press, 1967, pp. 78–79.
[13] S. Wolley, W. Brick, National Bureau of Standard, J. Res. 41 (1948) 470–472.
[14] James Larminie, Andrew Dicks, Fuel Cell Systems Explained, Wiley, New York, 2000, pp. 109–122.
[15] M.T. Ergul, et al., Int. Hydrogen Energy 22 (1997) 1039–1045.
[16] EG&G Services Parsons Inc., Fuel Cell Handbook, 5th ed., Science Applications International Corporation, 2000, pp. 4–6.